Principles and applications of broadband impulsive vibrational spectroscopy

M. Liebel, C. Schnedermann, T. Wende, and P. Kukura*

Physical and Theoretical Chemistry Laboratory, University of Oxford, South Parks Road, OX1 3QZ Oxford, UK.

E-mail: philipp.kukura@chem.ox.ac.uk

Abstract

We present an experimental setup for recording vibrational coherences and thereby Raman spectra of ground and excited electronic states over the 50-3000 cm^{-1} spectral range using broadband impulsive vibrational spectroscopy. Our approach relies on the combination of a sub-10 fs excitation pulse with an uncompressed whitelight continuum probe, which drastically reduces experimental complexity. We discuss the parameters determining vibrational coherence amplitudes and outline how to optimise the experimental setup including approaches aimed at conclusively assigning vibrational coherences to specific electronic states and provide a clear comparison with existing techniques. To demonstrate the applicability of our spectroscopic approach we conclude with several examples revealing the evolution of vibrational coherence in rhodopsin and β-carotene.

*To whom correspondence should be addressed

Introduction

Vibrational spectroscopy has contributed tremendously to our understanding of ultrafast light induced processes with infrared and Raman based approaches providing complimentary information about vibrational structural dynamics in molecules.[1–4] Infrared techniques have the advantage of directly measuring photon absorption and multi-dimensional implementations are now routine.[5] Raman-based methodologies[4,6,7] benefit from the ability of probing the full vibrational manifold of interest ranging from 50-3500 cm^{-1} and the potential for resonance enhancement of specific chromophore signatures. For nonlinear Raman spectroscopies, such as coherent anti-stokes Raman (CARS) and femtosecond stimulated Raman (FSRS), the temporal resolution is limited by the vibrational dephasing times,[8] but both techniques can achieve $\sim$ 20 fs temporal resolution with respect to the initiation of vibrational coherence (VC).

Time domain implementations of Raman spectroscopy, such as impulsive vibrational spectroscopy (IVS)[9–11] in principle provide similar information as that available in the frequency domain. Here, a short optical pulse initiates VC that, after computational Fourier transformation, yields a Raman spectrum of the molecule. A distinct advantage of impulsive over frequency domain Raman is that the full vibrationally coherent evolution of the system is measured. To extract information about chemical dynamics on time scales below vibrational dephasing times from a frequency domain measurement, it would be necessary to reconstruct the time dependent complex signal from the experimental data via the Kramers-Kronig relations. Imperfectly subtracted background signals, however, can cause line shape distortions, which inevitably introduce artefacts in the reconstructed data. If a time domain measurement is performed these artefacts are eliminated. IVS, for example, has been shown to be applicable to directly following chemical transformations with femtosecond time resolution.[12,13] Extensions of IVS towards complex molecular systems have, however, rarely been reported and were largely limited to the low frequency part of the vibrational spectrum, mainly due to the difficulties associated with pulse compression before the emergence

of commercially available chirped mirrors.[14,15]

In principle, time-domain vibrational spectroscopy has numerous advantages over frequency-domain based techniques. Of major importance is the fact that in the time-domain approach, the pulses generating and reading out the macroscopic polarisation are not overlapped in time. This avoids non-resonant background signals,[16] which have been plaguing non-linear Raman techniques for decades.[1,4] In addition, resonant IVS by definition takes advantage of resonance enhancement of the recorded optical signatures, a scenario that is frequently avoided in FSRS to suppress alternative and unwanted signal pathways.[17] A major drawback of IVS spectroscopy has been the difficulty of distinguishing ground and excited state vibrational coherence (VC) and the restricted spectral bandwidth accessible resulting in limited temporal resolution. Here, we show that many of these drawbacks are now easily addressed experimentally and that background-free ground and excited electronic state Raman spectra of very high signal-to-noise ratio can be recorded in the time-domain.

Principles of vibrational spectroscopy in the time domain

In the resonant description of IVS, an ultrashort broadband pump pulse in resonance with, for example, a ground-state electronic absorption band photoexcites the molecular system and impulsively generates VC on the excited electronic state (Figure 1a). The temporal evolution of the vibrational wavepacket causes spectral modulations of electronic transitions, such as stimulated emission (SE) or excited-state absorption (ESA).[18,19] A probe pulse following the pump pulse measures the transient absorption of the sample and, additionally, reveals any pump-induced time dependence of the SE or ESA signals. When probing a transient electronic band at a particular wavelength, the time dependent excited state signals result in oscillations at the frequencies of the initially excited coherent nuclear motion (Figure 1b). In this way, the oscillatory electronic response directly corresponds to the vibrational frequencies of the respective nuclear degrees of freedom and can be retrieved by Fourier transformation.

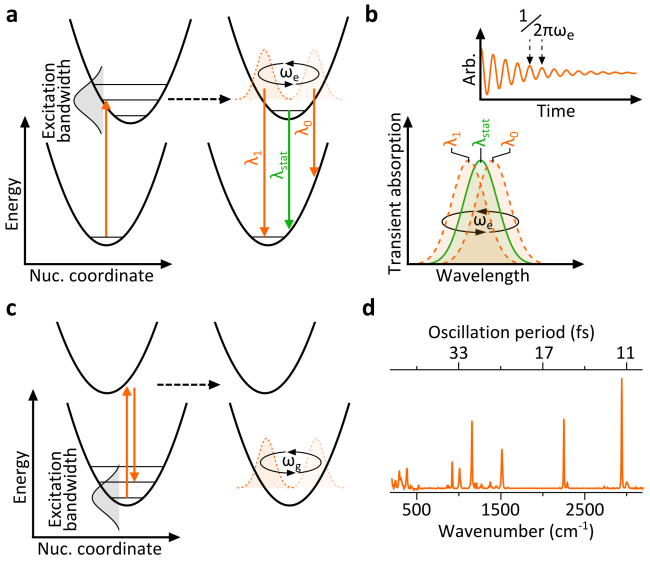

Figure 1: Concept of impulsive vibrational spectroscopy. (a) An ultrashort and thus spectrally broad pulse in resonance with an electronic transition generates vibrational coherence during photoexcitation. (b) The evolving VC manifests itself in a time dependent emission spectrum, which oscillates at the frequency corresponding to the energy difference of the superimposed vibrational eigenstates. (c) A pre-resonant pulse generates VC on the ground electronic state. (d) Comparison of oscillation periods and vibrational frequencies commonly encountered in organic molecules.

An ultrashort pulse, whether resonant or off-resonant with the electronic transition will also generate vibrational wavepackets on the ground state surface (Figure 1c) analogous to off-resonant Raman scattering in the frequency domain.[11,18,20] The concept is identical to that described above, except that the non-stationary vibrational state is located on the ground electronic state and the oscillatory electronic transient corresponds to modulations of the ground state absorption spectrum. This process has been termed impulsive stimulated Raman scattering (ISRS).[21,22] To facilitate the following discussions we will refer to it as off-resonant IVS. As in IVS, the VC can be recorded with a pump-probe (PP) experiment and yields information about the vibrational frequencies of the molecule under study, albeit in its ground electronic state. Both IVS and off-resonant IVS can be regarded as time domain implementations of nonlinear Raman spectroscopy.[23]

In order to implement IVS, sufficient bandwidth of the pump pulse is required to efficiently superimpose multiple vibrational eigenstates, while high temporal resolution is essential to

observe the VC experimentally. Frequency domain Raman spectra are commonly recorded in the 200-3500 cm^{-1} spectral range, corresponding to vibrational periods ranging from 170-10 fs, which in turn dictates the required temporal resolution (Figure 1d). For most applications, the most informative vibrational structural transitions are in the spectral region below 1700 cm^{-1} ($\tau_{vib} = 21$ fs), which is readily accessible with state-of-the-art ultrafast spectrometers. Especially the advent of commercially available chirped mirrors for pulse compression has drastically reduced the experimental hurdles associated with obtaining < 10 fs pulses.[24,25]

The emergence of array detectors with kilohertz readout rates enables spectrally dispersed detection of broadband probe pulses in a shot-to-shot fashion essential for high signal-to-noise measurements.[26] Such an approach not only provides spectral information over large energy bandwidths, but also circumvents the necessity to compress the probe pulse in order to achieve effective temporal resolutions approaching the transform-limit (TL).[27,28] Recently, we demonstrated on β-carotene, that a 12 fs pump pulse in combination with a broadband WL probe (BB-IVS) enables recording Raman spectra of the excited state, S_1, in the 100-1800 cm^{-1} spectral range with high signal-to-noise ratios exceeding the quality of state-of-the-art frequency domain techniques.[29–32] Two of the major advantages of this approach include that the probing is by definition resonantly enhanced and that the signal of interest is recorded without any temporal overlap of the excitation and detection pulses, reducing the influence of non-linear interfering background signatures.[33]

In the following sections we will discuss the experimental implementation of BB-IVS. We begin by considering off-resonant IVS to illustrate the key concepts and experimental requirements. We discuss how excited state VC, generated via IVS, can be distinguished from ground state contributions and conclude with an extension of these concepts towards recording time resolved vibrational kinetics by extending the two pulse experiment with a third, actinic pump pulse.

Experimental setup

A simplified scheme of a general BB-IVS setup is depicted in Figure 2. In our case, the light source is a Lightconversion Pharos-6W Yb:KGW amplifier providing 600 μJ of 200 fs pulses centered around 1030 nm at 10 kHz repetition rate, but analogous implementations based on more established Ti:Sapphire laser technology are possible.[34] Second-harmonic generation followed by sum-frequency generation yields pulses at 515 nm and 343 nm used to pump non-collinear optical parametric amplifiers (NOPAs)[35–37] to generate $<$ 10 fs pulses in the near-infrared (NIR) and in the visible (VIS) spectral range, respectively.[38]

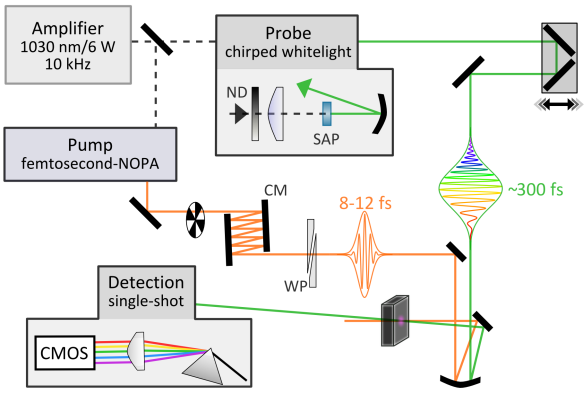

Figure 2: Schematic of an experimental setup for broadband impulsive vibrational spectroscopy with fundamental (black, dashed), probe (green) and pump (orange) beam paths. SAP = sapphire plate, ND = variable neutral density filter, CM = chirped mirrors, WP = wedge prisms.

Probe pulse generation

To generate the broadband probe pulse, we focus $\sim$ 3 μJ of the fundamental into a 3 mm sapphire plate using an F = 100 mm focal length achromatic lens. An F = 50 mm focal length curved mirror collimates the emerging probe and a harmonic separator (EKSMA Optics) isolates it from the residual fundamental. The uncompressed probe serves as a broadband probe pulse for all experiments presented in this manuscript. The use of reflective collimation is essential in minimising the chirp, thereby ensuring the highest possible effective

time resolution given finite spectral resolution in the detection.

Pump pulse generation

A detailed description of our NOPA designs has been reported previously.[38] Briefly, generation of < 10 fs pulses by means of a compression scheme based on a combination of prisms and gratings is a rather challenging task.[39] In our setup, we achieve compression of strongly chirped pulses (group velocity dispersion up to > 1500 fs^2 at 520 nm) to < 10 fs using chirped mirror pairs (Layertec GmbH). The experimental challenge when designing a NOPA for the generation of ultrashort pulses is thus no longer pulse compression but the amplification of sufficient bandwidth. Broadband amplification requires a relatively thin BBO crystal (1-2 mm) while operating the NOPA under broadband phase-matching conditions. It is furthermore necessary to minimise the chirp accumulated by the WL seed prior to amplification to enable temporal overlap of the maximum spectral amplification region with the pump pulse. This can be achieved by reducing the amount of material in the WL seed by means of reflective optics, omitting spectral filters and by employing a thin bulk material for initial WL generation. Operating the NOPA at low pump fluence reduces amplification-induced phase distortions and improves compressibility at the expense of output power. Above all, a spectrally uniform, high quality, WL seed is the key for the facile generation of < 10 fs pulses with close to TL durations.

Our NOPA designs are closely related to established schemes[37] with minor modifications required for the different pump wavelengths available with an Yb compared to a Ti:Sapphire source (Figure 3). Depending on the desired output wavelength, either the second (515 nm) or the third harmonic (343 nm) pumps the NOPA. We generate the WL seed by focusing 3 μJ of 1030 nm with an F = 100 mm focal length lens into a 3 mm sapphire plate. In our case, the temporal duration of 200 fs of both the 343 nm as well as the 515 nm pump pulses is long compared to other commercial laser systems. It might be necessary to employ thinner bulk materials for WL generation to reduce the chirp accumulated if shorter NOPA

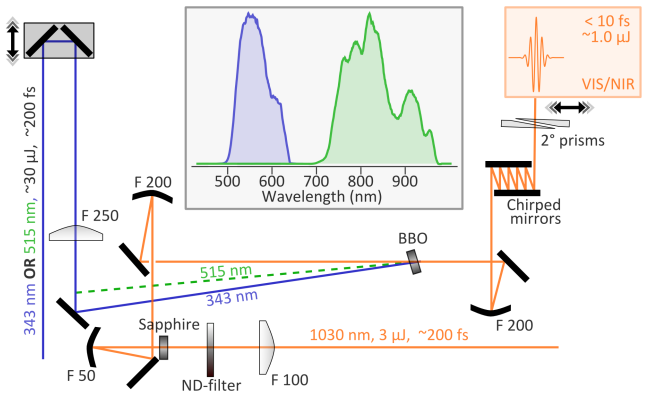

Figure 3: Schematic of a general NOPA design with typical pulse spectra obtained obtained using 343 (blue) and 515 nm (green) pumping.

pump pulse durations are used to maintain good temporal overlap with the full amplification bandwidth.[37] After collimation by a 50 mm focal length mirror, we focus the WL seed slightly in front of the BBO crystal with a 200 mm focal length mirror to obtain a diverging beam in the amplification crystal.

We commonly focus 30 μJ pump pulses with an F = 250 achromatic lens in front of the BBO crystal and temporally and spatially overlap them with the WL seed at an angle ensuring broadband phase-matching (2.5° or 4.2° internal angle at θ= 23.5° or θ = 37° for 515 nm and 343 nm operation, respectively). The crystal position is chosen such that a pump fluence of 150 GW/cm^2 is reached. The WL seed focus size is fine adjusted by means of the 50 mm focal length collimation mirror. As the mode of the WL seed becomes spectrally non-uniform towards the edges of the beam profile we found that hard aperture selecting the central region of the WL improves the NOPA output as we observe poor compressibility and extensive spatial chirp if the spectrally non-uniform part of the WL seed is amplified. The size of the WL in the BBO is adjusted to be smaller than the pump. In general, we operate our NOPAs at much lower conversion efficiencies (3 %) than achievable theoretically and reported previously in exchange for improved stability and mode quality. We remark that 1 μJ is still about an order of magnitude larger than the powers required for optical excitation in the linear regime for most samples.[40,41] After recollimation of the amplified

pulse by means of a 200 mm focal length mirror, a combination of chirped mirrors and thin fused silica wedges compresses the pulse close to the TL leading to < 10 fs pulses with corresponding broadband spectra (Figure 3). Given the very broad spectral bandwidth obtained from the NOPAs, tuning is rarely necessary as most samples can be excited by the same pulse.

The design presented here is optimised for 30 μJ of pump intensity with 200 fs pulses at either 343 or 515 nm. This design, however, is easily implemented with different parameters by following a few general considerations. If higher intensities are employed longer focal length focusing optics can be used which facilitate NOPA alignment due to the lower beam divergence.[31] The pump fluence within the crystal should be set to maximally 200 GW/cm^2 and the divergence of pump and WL seed inside of the crystal should be matched to ensure optimum performance. For pump wavelengths below 400 nm heating of the BBO crystal by 2 photon absorption has to be kept at acceptable levels and the pump fluence should hence be reduced below 200 GW/cm^2.[42]

Experimental implementation of BB-IVS

Pump and probe pulses are focused into the sample cell with an F = 200 mm focal length concave mirror and the probe is subsequently recollimated by an F = 500 mm focal length curved mirror before being directed into a home-built spectrograph. To avoid losses in the generally low intensity WL, we keep the number of optics in the detection path to a minimum. For dispersed detection, we employ a combination of a prism (SF11, 60° apex angle), an F = 60 mm NIR-achromatic doublet lens and a CMOS line camera (ISG LightWise LW-ELIS-1024A-1394) as a spectrometer. This configuration allows us to record the transmitted probe in the 480-950 nm spectral range with a spectral resolution exceeding 30 cm^{-1} close to the saturation limit of the camera (1 Me$^-$/px) with single-shot detection at 10 kHz readout. In this way, we can achieve shot-noise limited sensitivities of $<10^{-5}$ within 1 s of data acquisition on a day-to-day basis. We avoid the use of an entrance slit, compared to a Czerny-

Turner spectrograph, to minimise intensity noise caused by beam pointing fluctuations. Such an approach, however, requires spectral calibration prior to each measurement, which we perform by exploiting the strong spectral modulations of an FGB67-filter (Thorlabs or BG36, Schott).[41]

Data acquisition and processing

After spatially and temporally overlapping the compressed pump pulse with the chirped WL probe within the sample, we record differential absorbance spectra as a function of probe wavelength and pump-probe time delay as ($\mathrm{dOD}(\lambda, \Delta t)$) by modulating the pump pulse with a mechanical chopper:

$$\mathrm{dOD}(\lambda, \Delta t) = -\mathrm{Log}_{10}\left[\frac{\mathrm{ON}(\lambda, \Delta t)}{\mathrm{OFF}(\lambda)}\right],$$

with $\mathrm{ON}(\lambda, \Delta t)$ and $\mathrm{OFF}(\lambda)$ being the probe spectra recorded in the presence or absence of the pump pulse, respectively. By scanning the pump-probe delay we record the temporal evolution of the system after interaction with the pump pulse.

BB-IVS

Even though our main interest lies in recording VC of excited electronic states we will illustrate the main experimental concepts with data acquired in a completely off-resonant fashion. Solvents often exhibit only a few Raman active modes and we can therefore concentrate on the underlying principles of BB-IVS without the complications arising from congested Raman spectra of large polyatomic molecules. According to Figure 1 the observation of VC in a situation where both pump and probe pulses are far off-resonant, such as in organic solvents, should be impossible. Even though the pump pulse impulsively excites VC, the probe pulse fails to capture the resulting modulation as it is not probing the oscillating absorption spectrum. The synchronised molecular motion, however, induces a macroscopic polarisation

that modulates the refractive index and eventually the frequency content of the probe pulse. Depending on the pump-probe delay, the spectrum is either shifted towards higher or lower frequencies.[11,43] Importantly, the probe amplitude remains constant. If the probe pulse is detected in a spectrally unresolved fashion then this modulation remains undetected and other approaches are necessary to reveal their presence.[18] In spectrally-resolved detection the shifting probe spectrum is, however, readily observed in the transient signal. As BB-IVS intrinsically relies on the dispersed detection of an uncompressed WL, we will discuss the main concepts such as data acquisition and processing, effective time resolution and power dependencies with off-resonant systems.

BB-IVS on neat solvents

A differential absorbance map recorded on neat acetonitrile is presented in Figure 4a. Both the pronounced coherent artefact (CA) and the coherent oscillations reveal the chirp of the WL probe.[27,44] The first step in the data analysis is correcting the differential absorbance map for the wavelength dependent time zero caused by the probe chirp. A CA can be described analytically if longer pump pulses (> 30 fs) are used, but our experimental parameters often result in very complex CA shapes.[27] Especially for < 10 fs pulses in combination with a considerably chirped WL probe it is no longer feasible to describe the CA with analytical functions such as, for example, a sum of Gaussian derivatives. We found, however, that it is sufficient to fit the central part of the CA to a Gaussian function in order to retrieve the wavelength dependent time zero, which is defined as the center of the Gaussian. The validity of this approach is verified by retrieving the time zero from the phase of off-resonantly generated VC in a mixture of neat solvents. Even though the WL duration only marginally influences the effective temporal resolution, it is advantageous to nevertheless keep it to a minimum. Not only does the CA become increasingly complicated with increasing WL chirp, it furthermore broadens temporally, thereby contaminating the VC of interest.

Once the WL chirp is retrieved, the differential absorbance map can be corrected by

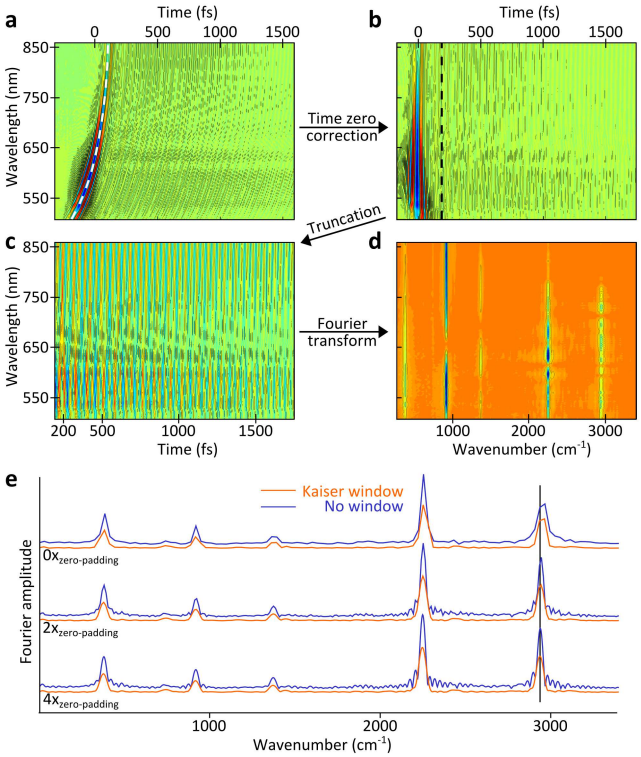

Figure 4: Extracting VC from a PP experiment recorded with a chirped WL probe. (a) Differential absorbance map recorded for acetonitrile in a 200 μm flow cell after off-resonant impulsive excitation with an 8 fs visible (550 nm) pump pulse and probing by a $\sim$ 300 fs chirped WL. The probe chirp retrieved from the coherent artefact is indicated in white, time zero is defined with respect to the carrier frequency of the probe. (b) Time zero corrected differential absorbance map obtained by interpolation of (a). (c) After truncation of the coherent artefact and exponential fitting of electronic kinetics pure VC is obtained. (d) Fourier transformation yields Raman spectra as a function of probe wavelength. (e) For truncated VC, the spectral quality after Fourier transformation can be improved by zero padding and the application of appropriate window functions. The vertical line indicates the correct Raman shift at 2941 cm^{-1} as determined by CW Raman spectroscopy.

means of wavelength dependent interpolation on a common time axis (Figure 4b). As the CA cannot be removed by analytical fitting, it is necessary to truncate the differential absorbance map in order to isolate the VC. Here, we truncated at t = 150 fs to confidently avoid any signal contamination by the CA (Figure 4c). We are left with pure VC, which after Fourier transformation on a wavelength by wavelength basis, reveals its wavelength dependent frequency content that can be conveniently represented in the form of a Fourier amplitude map (Figure 4d). Comparison with a Raman spectrum of acetonitrile recorded in the frequency domain allows us to identify the dominant bands of acetonitrile at 379, 919, 2254 and 2941 cm^{-1} throughout the detection window (530-860 nm).

The same data processing approach is valid for data recorded under resonant conditions: Time zero retrieval followed by time zero correction, CA truncation, exponential fitting of the electronic kinetics and Fourier transformation. It is advisable to independently record a CA on the neat solvent to facilitate the determination of the time zero, as electronic signals often mask the CA leading to an imperfect chirp correction. A perfect description of the the exponential decay kinetics is, in most cases, not required as the transient electronic signals are generally slow compared to most VC. Fitting imperfections hence manifest themselves as spectral distortion on the low wavenumber side of the vibrational spectrum (< 100 cm^{-1}) but do not distorted the high wavenumber regions. If information about low wavenumber VC is desired it is advisable to record temporally long transient absorption traces to facilitate fit convergence.

Fourier transformations, window functions and zero padding

Direct Fourier transformation of the VC is in principle sufficient to obtain detailed information about the frequency content. The spectral quality, however, markedly improves by post processing the experimental data.[45,46] Zero padding and the multiplication with a window function prior to Fourier transformation are the most common techniques. To illustrate the importance of zero padding we consider the differential absorbance map presented in Figure

4c. A total time range of t = 1551.2 fs (150 - 1701.2 fs) is recorded using $N = 554$ steps at a sampling interval of $\Delta t = 2.8$ fs. We compute the maximum resolvable frequency, or Nyquist frequency (ν_{Ny}), as half the sampling frequency (ν_{sam}):

$$\frac{\nu_{\mathrm{sam}}}{2} = \nu_{\mathrm{Ny}} = \frac{1}{2} \cdot \frac{1}{\Delta t \cdot c} \quad = \quad 5956.4\mathrm{cm}^{-1},$$

with c being the speed of light in vacuum. The spectral resolution, $\Delta\nu$, is computed as the ratio of ν_{sam} and the number of steps recorded, or directly from the acquisition time as:

$$\Delta\nu = \frac{\nu_{\mathrm{sam}}}{N} = \frac{1}{t \cdot c} = 21.5 \text{ cm}^{-1}.$$

The resulting Fourier spectra consist of $\frac{N}{2} = 277$ steps covering the spectral range from 0 to 5956.4 cm^{-1} in 21.5 cm^{-1} increments. Even though only five well-separated bands are present in each representative Fourier spectrum (Figure 4e) the actual frequencies are ill defined as a result of pixelation effects caused by insufficient data points covering the 5956.4 cm^{-1} of bandwidth. This can be improved by zero padding, as illustrated in Figure 4e. Initially, the band at 2941 cm^{-1} appears at the incorrect frequency due to spectral pixelation, but shifts upon increasing the length of the coherence vector by zero padding. Note, that the spectral resolution is solely determined by the total acquisition time, not the zero padding. Two coherences with a frequency separation smaller than $\Delta\nu$ can only be resolved by acquiring data over a longer time interval. Zero padding, however, leads to a smoother appearance of the Fourier spectrum.

The vector length increases to 9192 points with four zero pads as each individual zero pad extends the length to the next 2^n. The wavenumber spacing decreases to ~ 0.65 cm^{-1} and all bands appear at their correct wavenumbers, when compared with a frequency domain Raman spectrum. Pronounced ringing, however, appears in the vicinity of the bands as the VC is not sampled until it fully decays. In contrast, frequency domain Raman spectra are sampled

over the full coherence life-time, which results in Lorentzian line shapes. An identical Raman spectrum would be obtained in the time domain if the full temporal evolution of the VC was recorded, i.e. from time zero until the completion of the exponential decay. Sampling over a shorter time interval, as in our case ($t = 150.0 - 1701.2$ fs), effectively multiplies the full VC with a square window function which causes ringing after Fourier transformation. Seen from a Fourier perspective, the ringing corresponds to the line shape obtained after Fourier transformation of an exponential decay multiplied with a square window function. Initially, the ringing was not resolvable but upon decreasing the frequency spacing by zero padding it becomes visible in the spectrum. This ringing can be suppressed by multiplying the truncated VC with an additional window function thus altering the resulting line shape.

Figure 4e shows a comparison between the spectra obtained by zero padding only and a spectrum obtained after applying a Kaiser-Bessel window prior to zero padding. In the latter case the ringing is markedly suppressed. We found that a Kaiser-Bessel window is often well suited for applications in time domain Raman spectroscopy but refer to the extensive literature on this topic.[45] Especially when dealing with VC on short-lived electronic states the appropriate choice of a window function allows one to emphasise vibrational features that are difficult to observe in a frequency domain Raman spectrum as a result of the fast dephasing times resulting in broad, low amplitude, bands.

Probe duration and temporal resolution

An *a priori* surprising aspect of our methodology is the ability to resolve high frequency oscillations with vibrational periods as short as 11 fs (3000 cm^{-1}) with a probe pulse of nominal duration on the order of 300 fs. The use of a chirped WL probe has been addressed repeatedly in the literature, although never quantitatively at the effective temporal resolutions achieved here.[27,28] To provide a clear comparison between compressed and chirped WL probing we compare results obtained after compression with a deformable mirror placed in the Fourier plane of a 4f grating stretcher with those obtained with an uncompressed

probe pulse. By keeping the material in the WL to a minimum and furthermore slightly reducing the bandwidth to the 510-840 nm spectral range we are able to obtain a 4.5 fs (4.2 fs TL) WL probe, as characterized by SEA-TADPOLE.[47] The retrieved electric fields for both compressed and uncompressed WL probes are shown in their Wigner representations (Figure 5a).

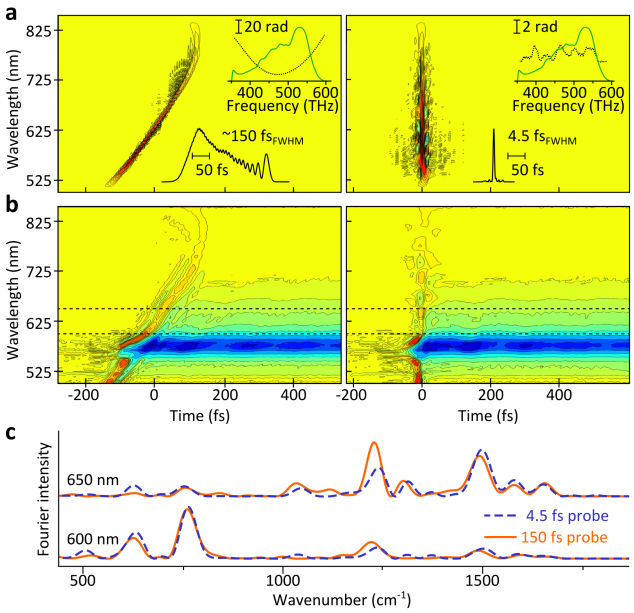

Figure 5: Chirped and compressed probing. (a) Wigner representations of chirped and compressed probe pulses. Inset: temporal and spectral pulse characterisation by means of SEA-TADPOLE. (b) Differential absorbance maps recorded for Rhodamine 101 in methanol using a 10 fs excitation pulse and a chirped (left) or compressed (right) WL probe. (c) Comparison of the Fourier intensity spectra obtained for the compressed (dashed) and chirped (solid) WL probes at 600 and 650 nm detection wavelength. The spectra were generated from the VC isolated by truncating the respective traces at t = 100 fs and subtracting the underlying electronic kinetics by means of exponential fitting.

The differential absorbance maps recorded with either chirped or compressed WL after photoexcitation of Rhodamine 101 dissolved in methanol with a 10 fs pulse are shown in Figure 5b. Before time zero, interference effects between pump and probe pulses manifest themselves in the low wavelength spectral region. Such effects are always present but are especially pronounced here due to the low WL intensity available after compression. The CA shapes strongly resemble the respective Wigner representations of the electric fields thus

emphasising the different phase terms of the two WL probes. The Fourier intensity spectra obtained for compressed and chirped probing show very good agreement despite the ∼30-fold difference in pulse duration (Figure 5c).

Parameters governing the vibrational coherence amplitude

Two electric field interactions with the pump pulse are necessary to generate VC and the VC amplitude therefore scales linearly with pump fluence as verified by an off-resonant BB-IVS experiment on neat chloroform (Figure 6a).[48] Figure 6b shows a comparison between experimentally obtained relative VC amplitudes, as a function of pump duration, for the most prominent Raman active modes in acetonitrile and the corresponding theoretical prediction obtained by convolving the respective oscillation with a Gaussian temporal profile prior to Fourier transformation. Especially high frequency modes exhibit a drastic decrease in VC amplitude with temporal resolution underlining why time domain observations of > 3000 cm^{-1} oscillations are rarely reported in the literature. The 1381 cm^{-1} mode represents a good indicator for the wavenumber region of interest and exhibits a moderate drop in amplitude with effective temporal resolution. As an example, doubling the pump duration from 8 to 16 fs results in a 75% relative decrease in VC amplitude for a 1500 cm^{-1} mode. Above all, effective temporal resolution is hence the key for any successful IVS experiment, but from our experience $\sim$ 12 fs pump pulses ensure sufficient VC amplitudes in most systems.

These results suggest that the probe duration does not influence the VC amplitude for spectrally dispersed detection with sufficient spectral resolution. The theoretical TL of the probe pulse, however, directly affects the coherence amplitude. We experimentally verify this prediction by spectrally filtering the probe pulse with a 4f-grating stretcher in combination with an adjustable slit in the Fourier plane. Reducing the available bandwidth, and hence increasing the TL of the probe, drastically influences the VC amplitude (Figure 6c). This finding can be rationalised by considering the following example: for a 10 fs pump pulse in combination with the broadband probe (TL $\sim$ 4 fs) we compute a maximum effective

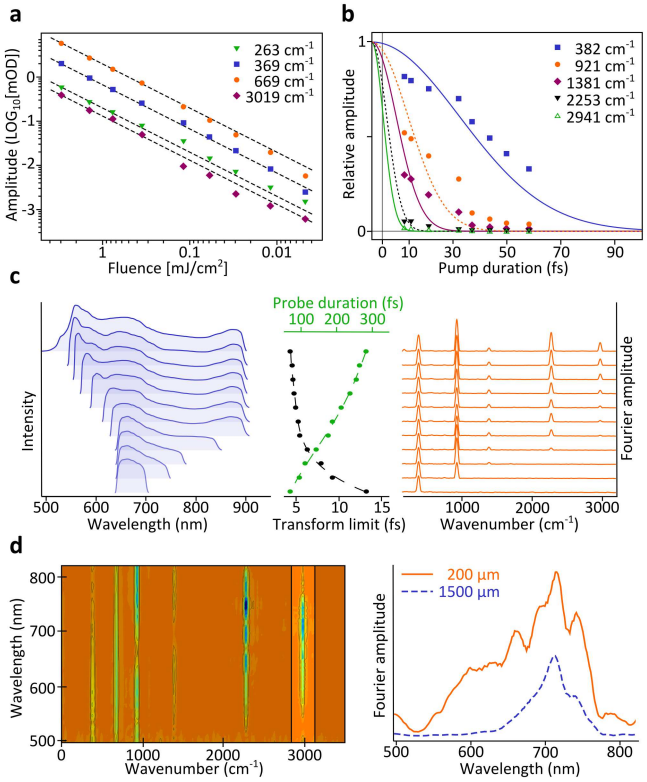

Figure 6: Experimental considerations for broadband impulsive vibrational spectroscopy. (a) Log-log plot of the pump power dependence of the VC amplitude recorded in neat chloroform (dots) using a 9.6 fs pump pulse centered at 520 nm and a chirped WL probe. The dashed lines indicate linear behavior. (b) Relative VC amplitude recorded as a function of pump duration for different vibrational modes in acetonitrile (dots) compared to a theoretical prediction(lines) assuming a 4 fs TL probe. (c) Left, probe spectra after narrowing the spectral bandwidth by means of a 4f-grating stretcher in combination with a hard aperture in the Fourier plane. Center, TL and duration of the probe pulses. Right, Fourier amplitude spectra obtained for acetonitrile by using the respective probe spectra (left) in combination with a 10 fs pump pulse centered at 570 nm. (d) Left, representative Fourier amplitude map recorded in 200 μm acetonitrile with a 6.9 fs pulse centered at 750 nm. Right, comparison of the wavelength dependent Fourier amplitude of the 2940 cm^{-1} band for 200 μm (solid) and 1500 μm (dashed) sample thickness, normalised to the number of sampled molecules.

temporal resolution of $\sqrt{4^2 + 10^2} = 10.8$ fs in the absence of all other effects. Reducing the probe bandwidth to a 10 fs TL lowers the temporal resolution to 14.4 fs thus reducing the VC amplitudes. As a result, it is not only convenient to employ non-amplified, uncompressed, broadband probe pulses, their use actually positively impacts on the effective temporal resolution, since amplification of parts of the WL continuum leads to a decrease in pulse bandwidth. In order to achieve the same effective temporal resolution (10.8 fs) with amplified and compressed pump and probe pulses one would have to employ two 7.5 fs pulses which is, from an experimental point of view, rather challenging.

Another important factor for optimising the coherence amplitude is the choice of flow-cell thickness. As pump and probe pulses pass through the sample they accumulate chirp and thus broaden temporally. As a consequence, a 12 fs TL pulse might yield better results than an 8 fs TL pulse as the temporal broadening is far less pronounced in the former due to the lower spectral bandwidth. Even more important is group-velocity mismatch (GVM) between pump and probe. When probing far from the excitation wavelength, GVM easily dominates, especially when employing sample thicknesses above 200 μm.

To illustrate the combination of both effects, we record a Fourier amplitude map for a 200 μm thick acetonitrile sample, contained in a flow-cell with 120 μm thick BK7 windows, with a 6.9 fs pump pulse centered at 750 nm (Figure 6d.). All expected vibrational modes up to 2941 cm^{-1} are observable. We then compare the 2941 cm^{-1} band amplitude to the one obtained for an identical experiment performed with 1500 μm of acetonitrile. After normalisation for the number of probed acetonitrile molecules we observe an overall reduction in VC amplitude. No GVM contributions are present in the spectral region of the pump pulse and the VC amplitude decrease is likely caused by chirping of the pump pulse while passing through the sample. Outside of the pump region GVM dominates, especially in the 1500 μm case where essentially all VC intensity for the high frequency stretch disappears. In a resonant experiment it is therefore advantageous to keep the flow cell thickness to a minimum while maintaining optical densities of > 0.3 if at all possible.

Off-resonant BB-IVS with resonant probing

Before discussing VC resulting from the photoexcitation of a molecule, it is instructive to consider off-resonantly excited VC in combination with resonant probing. In the case of an off-resonant probe, as for example in all the solvent experiments presented in the previous section, the wavelength dependent amplitude is strongly influenced by the probe spectrum and is generally non-trivial (see Figure 6d).[49] This situation changes for resonant probing as we are now recording the VC induced temporal modulation of the respective electronic transition as outlined in Figure 1. The wavelength dependence of the VC amplitudes should therefore follow the shape of the electronic absorption spectrum.[50]

To highlight this behavior, we perform an experiment on Nile Blue dissolved in methanol ($OD_{max} = 1$) using a 10 fs off-resonant pulse centered at 800 nm. We observe strong Raman activity slightly red shifted with respect to the ground state absorption maximum with most bands exhibiting at least one node within their wavelength dependent intensity distribution (Figure 7a). To rationalise these observations, we consider the schematic picture of an oscillating absorption spectrum presented (1b). In a differential transient absorption measurement, we would expect maximal coherence activity at positions where changes in the absorption spectrum are large. Here, a small shift of the absorption spectrum induces a large change in the differential signal. In contrast, in the vicinity of the absorption maximum the gradient is nearly zero resulting in a negligible VC amplitude and hence very small VC activity. We would thus expect most nodes around the absorption maximum of Nile Blue, or slightly red shifted as a result of the superposition of multiple vibrational energy levels.

Averaging the Fourier amplitude in the 510-700 nm region, followed by time resolution correction, results in the time domain Raman spectrum reported in Figure 7b.[52] Comparison with a resonance Raman spectrum recorded in the frequency domain shows very good agreement in both band frequencies and intensities.[51] Additionally, background fluorescence does not influence the results of the time-domain measurement as it merely causes slowly varying electronic signals which can be removed by exponential fitting. By recording Nile

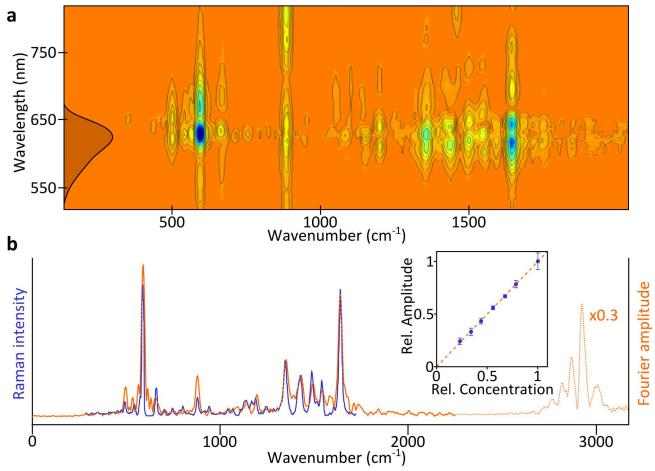

Figure 7: Impulsive vibrational spectroscopy with off-resonant pump and resonant probe. (a) Fourier amplitude map obtained for Nile Blue after off-resonant impulsive excitation of VC with a 10 fs pulse centered at 800 nm. Most of the coherence amplitude is localised near the Nile Blue absorption spectrum (inset). (b) Comparison of the time-corrected Fourier amplitude spectrum obtained by averaging the 510-700 nm region (orange) and a frequency domain resonance-Raman spectrum adapted from[51] (blue) show good agreement. Inset: Fourier amplitudes for different Nile Blue concentrations (blue dots) and linear fit (dashed, orange). The error bars indicate a 95 percent confidence interval.

Blue spectra at different dilutions we are able to confirm linear VC amplitude scaling with sample concentration (Figure 7b).

Resonant BB-IVS with resonant probing

Thus far we only generated and studied VC on ground electronic states. If the pump pulse is tuned into resonance with an electronic transition, we generate both ground and excited electronic state VC. To develop an understanding of the different signal contributions we compare experiments on Rhodamine 101 dissolved in methanol at low concentrations (OD = 0.3 in 200 μm path length) performed with resonant and off-resonant excitation. Using a 7.0 fs pump pulse centered at 790 nm, which is off-resonant with respect to the $S_1 \leftarrow S_0$ transition, ensures that no excited state population is generated. Only solvent and Rhodamine 101 ground state VC should be present in analogy with the Nile Blue experiment. Again, strong VC activity appears in proximity of the ground electronic state absorption spectrum (Figure

8a). The 1040 cm^{-1} band of methanol is visible over the full spectral range and demonstrates the spectrally non-trivial dependence of bands that are probed under off-resonant conditions.

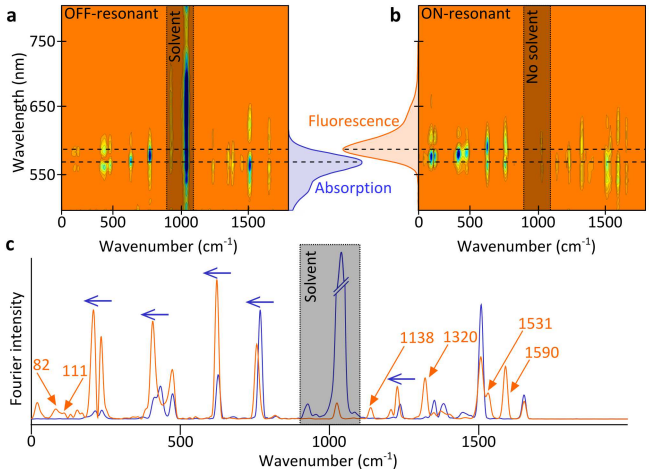

Figure 8: Monitoring vibrational coherence on ground and excited electronic states. (a) Fourier intensity map obtained for a BB-IVS experiment performed on Rhodamine 101 dissolved in methanol with an off-resonant pump pulse. The stationary absorption spectrum is indicated for comparison. (b) Fourier intensity map obtained with a pump pulse resonant with the $S_1 \leftarrow S_0$ electronic transition under otherwise identical conditions. The stationary fluorescence spectrum of Rhodamine 101 is shown for comparison. (c) Fourier intensity spectra for resonant (orange) and off-resonant (blue) pumping obtained by averaging the 530-650 nm region. The arrows indicate wavenumber shifts between on- and off-resonant pumping.

A shift of the pump pulse into resonance with the $S_1 \leftarrow S_0$ transition (8.9 fs centered at 540 nm) results in only subtle changes of the Fourier intensity map (Figure 8b). The methanol band (1040 cm^{-1}) vanishes, indicating that the probability of VC generation in Rhodamine 101 under resonant pumping is enhanced compared to the solvent. A comparison of the two experiments suggests that resonant excitation causes an even larger red shift of the VC activity compared to the ground state absorption spectrum. Previously, we explained the slight red shift of ground state VC by the superposition of multiple vibrational eigenstates, which reduces the effective S_0-S_1 energy gap. Photoexcitation of Rhodamine 101 generates VC in the $S_1 \rightarrow S_0$ SE region. The superposition of vibrational eigenstates in the excited electronic state increases the S_0-S_1 energy gap and thus results in a blue shift of Fourier intensities with respect to the SE spectrum. Revisiting Figure 8b indeed reveals a blue-

shift of most of the Fourier intensity nodes with respect to the fluorescence spectrum of Rhodamine 101. These observation lead us to conclude that VC on the excited electronic state dominates the Fourier intensity map obtained under resonant pumping conditions. The differences in the wavelength dependent amplitudes are, however, subtle. Especially if only the resonant experiment would have been performed, a conclusive assignment of the VC to either the ground or excited electronic state would be difficult.

Raman intensities are always a function of the pulses interacting with the system.[53,54] The vibrational frequencies, however, are solely a function of the molecular system itself. Averaging the 530-650 nm spectral region of the Fourier intensity maps allows us to compare the spectral features obtained under on- and off-resonant conditions (Figure 8c). We indeed observe clear differences between the two spectra. Almost all bands present under off-resonant pumping disappear from the spectrum and are replaced by several new bands as well as multiple bands of slightly shifted frequencies. For example, new bands appear at 1138, 1320, 1531 and 1590 cm^{-1} and all features in the 200-800 cm^{-1} spectral region exhibit frequency shifts when moving from off- to on-resonant pumping.

Taken together, we see clear indications for the efficient generation of excited state VC in Rhodamine 101 under resonant pumping. Due to the small Stokes shift of the fluorescence signal with respect to the ground state absorption spectrum as well as the spectral similarity of ground and excited electronic state VC, conclusive isolation of excited electronic state VC remains difficult. Experiments under on- and off-resonant pumping conditions in combination with spectrally broad probing windows does, however, allow us to assign most of the vibrational modes observed to the excited electronic state of Rhodamine 101. We note that it is possible to selectively isolate pure excite state VC by employing a third, dump pulse, as discussed in detail previously.[55]

Time domain Raman of excited electronic states

The Rhodamine 101 example showcased the ability of BB-IVS to create and monitor excited electronic state VC but also underlined the difficulties associated with its identification. We will now present two systems where excited state VC could be confidently identified solely based on their temporal and wavelength dependent behavior.

Vibrational coherence in the photoproduct of an isomerisation reaction

After photoexcitation of the protein rhodopsin (rho), the 11-*cis* retinal protonated Schiff base chromophore isomerises to the all-*trans* configuration within $\sim$ 200 fs to form the primary photoproduct bathorhodopsin (Figure 9a).[56,57] We record a differential absorbance map to follow the electronic evolution of rho after excitation with an 8 fs pulse centered at 500 nm in resonance with the $S_1 \leftarrow S_0$ transition.[58] Around time zero, the signal is dominated by strong CA contributions quickly followed by a rapidly red shifting SE signature (800 nm), which leaves the spectral detection window towards the NIR and reappears as photoinduced absorption of the isomerisation product (Figure 9b). The photoproduct signature cools and approaches a stationary transient spectrum centered at 560 nm over the duration of our temporal detection window. VC signatures superimposed onto the electronic kinetics are clearly visible in the differential absorbance map.

Isolating the VC from t = 80 fs, as outlined earlier, reveals the underlying VC activity, which is almost exclusively present in the spectral region of rho and bathorhodopsin (Figure 9b). To determine the origin of the VC, we compare the frequency content of the 570-640 nm spectral region to the VC activity obtained under off-resonant excitation conditions (9 fs pump centered at 800 nm) as previously for Rhodamine 101 (Figure 9c).

Under resonant conditions we find strong VC in the torsional (< 500 cm^{-1}), hydrogen-out-of-plane (800-1100 cm^1), C-C stretching (1150-1350 cm^1), and the C=C stretching (1500-

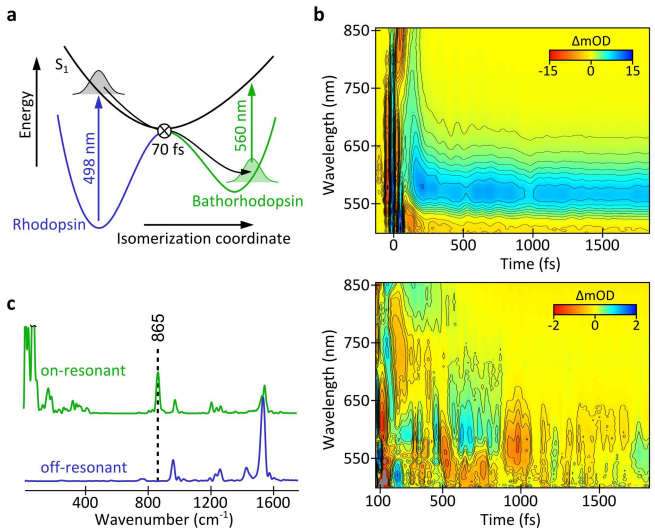

Figure 9: Vibrationally coherent isomerisation of rhodopsin (rho) following resonant excitation. (a) Simplified, 1-dimensional reaction coordinate of rhodopsin. (b) Differential absorbance map recorded for rho after photoexcitation with an 8 fs pump pulse centered at 500 nm and residual VC obtained after truncation and fitting of the differential absorbance map. (c) Comparison of Fourier intensity spectra obtained by averaging the 570-640 nm spectral range for both resonant (green) and off-resonant (blue) excitation.

1650 cm[1]) regions with wavenumbers matching those reported for bathorhodopsin.[3,59] The off-resonant experiment reproduces the resonance Raman spectrum of rho and is lacking the pronounced low frequency activity as well as the 865 cm^{-1} hydrogen-out-of-plane wagging mode. We note that even the intensity distribution of the three major bands present in the $1150 - 1350$ cm[1] region changes when moving from on- to off-resonant excitation conditions. These observations suggest that the photoisomerisation of rhodopsin proceeds in a vibrationally coherent fashion.[58,60,61] In contrast to data recorded on the same isomerisation with FSRS,[3] our time-domain approach does not appear to be capable of revealing time-dependent changes in vibrational coherences occurring on a time-scale shorter than the vibrational dephasing time.[58]

Evolution of vibrational coherence during ultrafast electronic internal conversion

Photoexcitation in resonance (12 fs pump centered at 480 nm) with the lowest energy one-photon allowed transition of β-carotene in toluene populates the S_2 electronic state, which rapidly internally converts into S_1 (Figure 10a).[62,63] A differential absorbance map following the electronic kinetics is presented in Figure 10b. The early time delays (<100 fs) are dominated by the CA, rapidly followed by ESA from S_2 in the NIR spectral region. The rise of S_1 ESA at 570 nm, concomitant with the decay of S_2 ESA, proceeds with the same time constant of 140 fs.

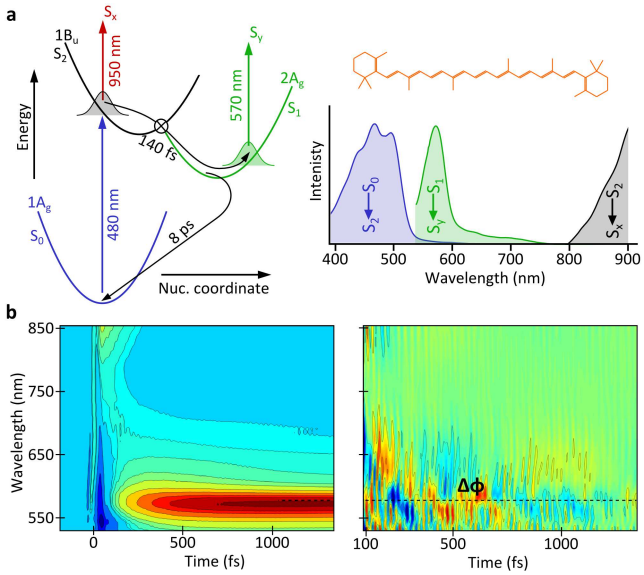

Figure 10: Internal conversion in β-carotene proceeds in a vibrationally coherent fashion. (a) Potential energy scheme of β-carotene dissolved in toluene and absorption spectra of the three energetically lowest lying singlet states. (b) Left, differential absorbance map recorded on β-carotene after photoexcitation with a 12 fs pump pulse centered at 480 nm. Right, residual VC after truncating the map at t = 85 fs followed by removal of the electronic kinetics by means of exponential fitting. The dashed line is a guide to the eye indicating the spectral region phase jump ($\Delta\phi$) of the oscillations,

We isolate the VC by truncating the differential absorbance map at t = 85 fs followed by fitting the underlying electronic kinetics with a model consisting of two exponentially decaying functions. The residual VC exhibits regions of pronounced coherence activity (Figure

10b). Short-lived VC is evident in the S_2 ESA region and VC with a considerably longer lifetime is present in the spectral region of the S_1 ESA. In fact, we observe a phase jump in the VIS spectral region around the absorption maximum of the first excited electronic state. Based on its drastically reduced lifetime, we assign the NIR VC to originating from S_2. The long-lived VC in the S_1 spectral region exhibits a phase jump that is slightly red shifted compared to the S_1 ESA transition. A phase jump can be rationalised by considering the notion of a temporally moving absorption spectrum (Figure 1b) and leads, upon Fourier transformation, to the intensity nodes observed in the Fourier maps of Rhodamine 101 or Nile Blue. The wavelength dependent nature of the VC thus suggests that they originate from S_1.

The spectral content of the VC does indeed reveal well-known S_1 Raman bands but we note that contamination with both solvent and ground electronic state VC is present throughout the spectrum. As discussed in detail elsewhere[55,64] it is, however, possible to selectively isolate the excited state VC by employing an additional pulse for electronic population control .

Time-resolved Raman spectroscopy

So far, we have shown that it is possible to create and follow VC on both ground and excited electronic states. If one is interested in vibrational kinetics, however, it is necessary to record Raman spectra of an evolving system at different points in time. To conclude, we thus present a three pulse extension that is conceptually similar to techniques such as time resolved resonance Raman or FSRS. A pump pulse, often termed actinic pulse, triggers a photo-reaction by exciting molecules from the ground to an electronically excited state. Impulsive Raman then follows the vibrational evolution of the photo excited molecules as a function of time delay between the actinic pulse and the Raman probe pulse(s).

To showcase that time domain Raman is well-suited for recording ultrafast vibrational

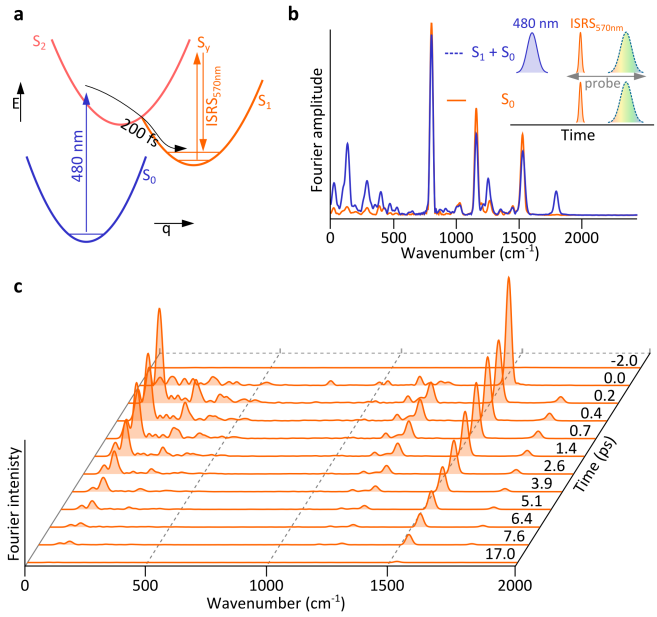

Figure 11: Time resolved time domain Raman on the S_1 state of β-carotene in toluene. (a) Electronic states and dynamics of β-carotene. (b) Pulse schemes for acquisition of time resolved vibrational dynamics and Raman spectra obtained after Fourier transformation of the VC recorded in the 520-600 nm spectral region in the presence (blue) and the absence (orange) of an actinic pulse (solvent bands have been subtracted for clarity). (c) Temporal evolution of the S_1 Fourier intensity spectrum as a function of actinic to impulsive pulse delay.

dynamics we chose the well studied system β-carotene. A 200 fs actinic pulse centered at 480 nm excites β-carotene into S_2 via a one-photon transition (Figure 11a). The S_2 population rapidly decays within $\sim$ 140 fs into S_1 via a conical intersection. After a variable time delay, an impulsive pump pulse resonant with the $S_y \leftarrow S_1$ ESA transition creates VCs in both the S_1 and the S_0 electronic state, which is consecutively probed by a WL continuum. By modulating the actinic pulse we are able to record VC in both a mixture of ground and excited state molecules and for ground state molecules only (Figure 11b). The vibrational spectra obtained after Fourier transformation of the VC thus either consist of only ground state or a mixture of ground and first excited electronic state bands. Subtraction of the scaled ground electronic state only VC, as well as any solvent VCs, allows for the isolation of pure excited electronic state VC and hence Raman spectra.

By changing the actinic-impulsive pulse to WL probe time delay we are able to follow the vibrational evolution of β-carotene in its first excited electronic state, results of which are shown in Figure 11c. We observe a signal rise within our instrument response function of $\sim$ 200$\pm$20 fs followed by an exponential decay of 6.1$\pm$0.4 and 5.8$\pm$0.3 ps for the 1538 and 1785 cm^{-1} bands which is in good agreement with previous reports.[65–68] As previously mentioned, an alternative approach is to use an additional depletion pulse to directly isolate the excited state VC.[55] Here, a temporally long pulse is tuned into resonance with an electronic transition originating from the excited state of interest to selectively remove population and with it VC amplitude. A direct subtraction of VC recorded in the presence and absence of this dump pulse isolates the VC of interest.

The excited state spectra presented in Figure 11c were acquired using β-carotene dissolved in toluene at an optical density of OD = 1 and exhibit signal levels of around 100 μOD. We integrated for 10 min/spectrum at 10 kHz and used an 80 nJ impulsive pulse (8.2 fs, 70x67 μm focus at FWHM) and 520 nJ of a 515 nm actinic pump (200 fs, 150x90 μm focus at FWHM) in combination with a 55x55 μm (focus at FWHM) WL probe. Identical signal magnitudes are obtained with a fully resonant actinic pump with powers below 100 nJ.

Conclusion and outlook

We have discussed how a transient absorption setup with high temporal resolution and sensitivity can record VCs in the time domain over a large frequency bandwidth. The combination of an ultrashort excitation pulse with a broadband WL continuum probe reduces the experimental complexity and improves the signal-to-noise, while simultaneously ensuring optimal effective temporal resolution. Even though most of the discussion of experimental parameters was limited to off-resonant systems such as neat solvents, the concepts are directly applicable to molecules studied with resonant excitation.

Our time domain implementation of vibrational spectroscopy has three major advantages over frequency domain approaches: (i) It is possible to initiate VC on a reactive potential energy surface with the photoexcitation pulse and hence address questions on how photon energy is coherently converted into nuclear and electronic motion.[52] (ii) The issue of non-trivial baselines frequently encountered in frequency domain Raman spectroscopy is entirely absent if the VC is recorded in the time domain. It is hence possible to obtain high-quality Raman spectra of any electronic state of interest even under fully resonant excitation and probing conditions of strongly fluorescing molecules as illustrated for Rhodamine 101 and Nile Blue. (iii) Generation of 10 fs pulses from a standard fs amplifier system is today experimentally much less demanding than the generation of tunable picosecond pulses as required for frequency domain techniques. Finally, it is possible to extend any of these experiments with an additional population control pulse to directly obtain excited state only Raman spectra and hence remove ambiguities associated with the electronic origin of the studied coherences.[55] To which degree the results obtained in this fashion are similar or different to those involving non-dispersed detection[34] will require more experimental but mostly theoretical insight. Irrespective, BB-IVS enables background-free resonantly enhanced recording of ground and excited state Raman spectra with high SNR and an easily implementable experimental setup

Acknowledgement

References

(1) Hamaguchi, H.; Gustafson, T. *Annu. Rev. Phys. Chem.* **1994**, *45*, 593–622.

(2) Nibbering, E. T. J.; Fidder, H.; Pines, E. *Annu. Rev. Phys. Chem.* **2005**, *56*, 337–367.

(3) Kukura, P.; McCamant, D. W.; Yoon, S.; Wandschneider, D. B.; Mathies, R. A. *Science* **2005**, *310*, 1006–1009.

(4) Kukura, P.; McCamant, D. W.; Mathies, R. A. *Annu. Rev. Phys. Chem.* **2007**, *58*, 461–88.

(5) Fayer, M. D. *Annu. Rev. Phys. Chem.* **2009**, *60*, 21–38.

(6) Schmitt, M.; Knopp, G.; Materny, A.; Kiefer, W. *Chem. Phys. Lett.* **1997**, *270*, 9–15.

(7) Bell, E. J. S. *Anaylst* **1996**, *121*, 107R–120R.

(8) Mukamel, S.; Biggs, J. D. *J. Chem. Phys.* **2011**, *134*, 161101(R).

(9) De Silvestri, S.; Fujimoto, J. G.; Ippen, E. P.; Gamble, E. B.; Williams, L. R.; Nelson, K. A. *Chem. Phys. Lett.* **1985**, *116*, 146–152.

(10) Yan, Y.-X.; Gamble, E. B.; Nelson, K. A. *J. Chem. Phys.* **1985**, *83*, 5391–5399.

(11) Ruhman, S.; Joly, A. G.; Nelson, K. A. *IEEE J. Quantum Elect.* **1988**, *24*, 460–469.

(12) Rose, T. S.; Rosker, M. J.; Zewail, A. H. *J. Chem. Phys.* **1988**, *88*, 6672–6673.

(13) Zewail, A. H. *J. Phys. Chem. A* **2000**, *104*, 5660–5694.

(14) Zhu, L.; Sage, J. T.; Champion, P. M. *Science* **1994**, *266*, 629–632.

(15) Takeuchi, S.; Tahara, T. *J. Phys. Chem. A* **2005**, *109*, 10199–10207.

(16) Kamga, F. M.; Sceats, M. G. *Opt. Lett.* **1980**, *5*, 126.

(17) McCamant, D. W.; Kukura, P.; Mathies, R. A. *J. Phys. Chem. B* **2005**, *109*, 10449–10457.

(18) Dhar, L.; Rogers, J. A.; Nelson, K. A. *Chem. Rev.* **1994**, *94*, 157–193.

(19) Mukamel, S. *Physics-Uspekhi*; 1995.

(20) Walmsley, I. A.; Tang, C. L. *J. Chem. Phys.* **1990**, *92*, 1568–1574.

(21) Robinson, M. M.; Yan, Y.-X.; Gamble, E. B.; Williams, L. R.; Meth, J. S.; Nelson, K. A. *Chem. Phys. Lett.* **1984**, *112*, 491–496.

(22) Chesnoy, J.; Mokhtari, A. *Phys. Rev. A* **1988**, *38*, 3566–3576.

(23) Johnson, A. E.; Myers, A. B. *J. Chem. Phys.* **1996**, *104*, 2497–2507.

(24) Szipocs, R.; Ferencz, K.; Spielmann, C.; Krausz, F. *Opt. Lett.* **1994**, *19*, 201–203.

(25) Zavelani-Rossi, M.; Cerullo, G.; De Silvestri, S.; Gallmann, L.; Matuschek, N.; Steinmeyer, G.; Keller, U.; Angelow, G.; Scheuer, V.; Tschudi, T. *Opt. Lett.* **2001**, *26*, 1155–1157.

(26) Polli, D.; Lüer, L.; Cerullo, G. *Rev. Sci. Instrum.* **2007**, *78*, 103108.

(27) Kovalenko, S. A.; Dobryakov, A. L.; Ruthmann, J.; Ernsting, N. P. *Phys. Rev. A* **1999**, *59*, 2369–2384.

(28) Polli, D.; Brida, D.; Mukamel, S.; Lanzani, G.; Cerullo, G. *Phys. Rev. A* **2010**, *82*, 053809(R).

(29) Liebel, M.; Kukura, P. *J. Phys. Chem. Lett.* **2013**, *4*, 1358–1364.

(30) Shim, S.; Mathies, R. A. *J. Phys. Chem. B* **2008**, *112*, 4826–4832.

(31) Kovalenko, S. A.; Dobryakov, A. L.; Ernsting, N. P. *Rev. Sci. Instrum.* **2011**, *82*, 063102.

(32) Zhu, L.; Liu, W.; Fang, C. *Appl. Phys. Lett.* **2014**, *105*, 041106.

(33) Dudovich, N.; Oron, D.; Silberberg, Y. *Nature* **2002**, *418*, 512–514.

(34) Fujisawa, T.; Kuramochi, H.; Takeuchi, S.; Tahara, T. *Springer Proc. Phys.* **2015**, *162*, 539–543.

(35) Wilhelm, T.; Piel, J.; Riedle, E. *Opt. Lett.* **1997**, *22*, 1494–1496.

(36) Cerullo, G.; Nisoli, M.; Stagira, S.; De Silvestri, S. *Opt. Lett.* **1998**, *23*, 1283–1285.

(37) Cerullo, G.; De Silvestri, S. *Rev. Sci. Instrum.* **2003**, *74*, 1–18.

(38) Liebel, M.; Schnedermann, C.; Kukura, P. *Opt. Lett.* **2014**, *39*, 4112–4115.

(39) Fork, R. L.; Brito Cruz, C. H.; Becker, P. C.; Shank, C. V. *Opt. Lett.* **1987**, *12*, 483–485.

(40) Homann, C.; Schriever, C.; Baum, P.; Riedle, E. *Opt. Express* **2008**, *16*, 5746–5756.

(41) Megerle, U.; Pugliesi, I.; Schriever, C.; Sailer, C. F.; Riedle, E. *Appl. Phys. B-Lasers O.* **2009**, *96*, 215–231.

(42) Bradler, M.; Riedle, E. *Opt. Lett.* **2014**, *39*, 2588–2591.

(43) Banin, U.; Bartana, A.; Ruhman, S.; Kosloff, R. *J. Chem. Phys.* **1994**, *101*, 8461–8481.

(44) Dobryakov, A. L.; Kovalenko, S. A.; Ernsting, N. P. *J. Chem. Phys.* **2003**, *119*, 988–1002.

(45) Harris, F. *P. IEEE* **1978**, *66*, 51–83.

(46) Stoica, P.; Moses, R. *Spectral analysis of signals*; 2005.

(47) Bowlan, P.; Gabolde, P.; Shreenath, A.; McGresham, K.; Trebino, R.; Akturk, S. *Opt. Express* **2006**, *14*, 11892–11900.

(48) Lee, S.-Y.; Heller, E. J. *J. Chem. Phys.* **1979**, *71*, 4777–4788.

(49) Pollard, W. T.; Mathies, R. A. *Annu. Rev. Phys. Chem.* **1992**, *43*, 497–523.

(50) Kobayashi, T.; Wang, Z. *IEEE J. Quantum Elect.* **2008**, *44*, 1232–1241.

(51) Lawless, M. K.; Mathies, R. A. *J. Chem. Phys.* **1992**, *96*, 8037–8045.

(52) Liebel, M.; Schnedermann, C.; Bassolino, G.; Taylor, G.; Watts, A.; Kukura, P. *Phys. Rev. Lett.* **2014**, *112*, 238301(R).

(53) Pollard, W. T.; Dexheimer, S. L.; Wang, Q.; Peteanu, L. A.; Shank, C. V.; Mathies, R. A. *J. Phys. Chem.* **1992**, *96*, 6147–6158.

(54) Dobryakov, A. L.; Ernsting, N. P. *J. Chem. Phys.* **2008**, *129*, 184504(R).

(55) Wende, T.; Liebel, M.; Schnedermann, C.; Pethick, R. J.; Kukura, P. *J. Phys. Chem. A* **2014**, *118*, 9976–9984.

(56) Schoenlein, R. W.; Peteanu, L. A.; Mathies, R. A.; Shank, C. V. *Science* **1991**, *254*, 412–415.

(57) Polli, D.; Altoè, P.; Weingart, O.; Spillane, K. M.; Manzoni, C.; Brida, D.; Tomasello, G.; Orlandi, G.; Kukura, P.; Mathies, R. A.; Garavelli, M.; Cerullo, G. *Nature* **2010**, *467*, 440–443.

(58) Schnedermann, C.; Liebel, M.; Kukura, P. *J. Am. Chem. Soc.* **2015**, *137*, 2886–2891.

(59) Lin, S. W.; Groesbeek, M.; van der Hoef, I.; Verdegem, P.; Lugtenburg, J.; Mathies, R. A. *J. Phys. Chem. B.* **1998**, *102*, 2787–2806.

(60) Wang, Q.; Schoenlein, R. W.; Peteanu, L. A.; Mathies, R. A.; Shank, C. V. *Science* **1994**, *266*, 422–424.

(61) Köppel, H.; Domcke, W.; Cederbaum, L. S. *Adv. Chem. Phys.* **1984**, *57*, 59–246.

(62) Polívka, T.; Sundström, V. *Chem. Rev.* **2004**, *104*, 2021–2071.

(63) Pérez Lustres, J. L.; Dobryakov, A. L.; Holzwarth, A.; Veiga, M. *Angew. Chem. Int. Ed.* **2007**, *46*, 3758–3761.

(64) Liebel, M.; Schnedermann, C.; Kukura, P. *Phys. Rev. Lett.* **2014**, *112*, 198302(R).

(65) McCamant, D. W.; Kim, J. E.; Mathies, R. A. *J. Phys. Chem. A* **2002**, *106*, 6030–6038.

(66) McCamant, D. W.; Kukura, P.; Mathies, R. A. *J. Phys. Chem. A* **2003**, *107*, 8208–8214.

(67) Kraack, J. P.; Wand, A.; Buckup, T.; Motzkus, M.; Ruhman, S. *Phys. Chem. Chem. Phys.* **2013**, *15*, 14487–14501.

(68) Takaya, T.; Iwata, K. *J. Phys. Chem. A* **2014**, *118*, 4071–4078.

Graphical TOC Entry